MTLA 30 (2023) 101847

Contents lists available at ScienceDirect

Materialia

journal homepage: www.elsevier.com/locate/mtla

Full length article

Observation of long-range anisotropy in a vapor-deposited metallic glass

Peihao Sun [a,*], Alessandro Martinelli [a], Alexey P. Melnikov [b], Manfred Burghammer [b], Jerzy Antonowicz [c], Ryszard Sobierajski [d], Paul Fuoss [e], Alfred Q.R. Baron [f], Kenji Tamasaku [g], Hiroyuki Ohsumi [g], Federico Caporaletti [h], Jussi-Petteri Suuronen [i,b], Rémi Tucoulou [b], Konrad Samwer [j], J.B. Hastings [e,*], Giulio Monaco [a,*]

[a] Dipartimento di Fisica e Astronomia "Galileo Galilei", Università degli Studi di Padova, Via F. Marzolo, 8, Padova, 35131, PD, Italy
[b] ESRF, The European Synchrotron, 71 Avenue des Martyrs, CS40220, Grenoble, 38043 Cedex 9, France
[c] Faculty of Physics, Warsaw University of Technology, Koszykowa 75, Warsaw, 00-662, Poland
[d] Institute of Physics Polish Academy of Sciences, al. Lotników 32/46, Warsaw, 02-668, Poland
[e] SLAC National Accelerator Laboratory, 2575 Sand Hill Rd, Menlo Park, 94025, CA, USA
[f] Materials Dynamics Laboratory, RIKEN SPring-8 Center, Sayo, 679-5148, Hyogo, Japan
[g] RIKEN SPring-8 Center, Sayo, 679-5148, Hyogo, Japan
[h] Laboratory of Polymer and Soft Matter Dynamics, Experimental Soft Matter and Thermal Physics (EST), Université libre de Bruxelles (ULB), Brussels, 1050, Belgium
[i] Xploraytion, Bismarckstrasse 10-12, Berlin, 10625, Germany
[j] I. Physikalisches Institut, University of Goettingen, Goettingen, 37077, Germany

ARTICLE INFO

Keywords:
Metallic glass
X-ray diffraction
Physical vapor deposition
Ordering
X-ray nanofocus

ABSTRACT

The mesoscopic structure of amorphous materials remains to be understood. Although amorphous systems are often thought to be randomly structured beyond short-range ordering, a number of studies reveal the importance of medium-range ordering up to a few nanometers. Here, using a newly available high-flux nano-focused X-ray beam, we observe anisotropy in a vapor-deposited PdCuSi metallic glass even in a large probed volume of around 60 nm × 60 nm × 5 μm. With annealing, the anisotropy disappears without crystallization. The observations allow us to exclude alternative explanations including geometric and strain effects, leading to the conclusion that the anisotropy must arise from structural correlations. Our results suggest that anisotropy may persist even to macroscopic scales in amorphous materials, pointing out the need for structural descriptions of glasses beyond isotropic pair correlation functions as well as the possibility to realize glassy structures with long-range correlations.

Despite decades of research, the structure of amorphous materials is not yet fully understood. Traditionally, glasses are thought to be built of a random arrangement of atoms or molecules respecting certain short-range ordering (SRO). Widely used models include the continuous random network model [1] for network glasses and the dense random packing model [2] for metallic glasses. Recently, these models have been challenged by new experimental evidence [3,4]. In particular, for metallic glasses, a number of works have confirmed the existence of medium-range ordering (MRO), i.e., ordered structures from beyond the first coordination shell to 1–2 nm, which can have significant effects on their physical properties [5]. Some studies have revealed structural correlations persisting to even longer ranges. For example, topological and chemical ordering up to 4–6 nm in $ZrCl_2$ and $GeSe_2$ glasses have been reported [6]. Local ordering with correlation lengths up to 5–6 nm has also been found in PdNiP samples with minor alloying (i.e., with the addition of a small amount of alloying elements) [7], a nice confirmation of the fact that adding less than a percent of alloying elements can substantially change various properties of metallic glasses [7,8]. On larger length scales, although there is evidence suggesting the existence of long-range topological ordering in a $Ce_{75}Al_{25}$ metallic glass [9], to our knowledge, direct proof for long-range structural correlations has not yet been found. Instead, the structure of amorphous materials is generally thought to be uniform. Even if MROs are present, they are usually assumed to be randomly distributed within the sample without any long-range correlation. In addition, most structural characterizations and descriptions of glasses to date make use of radial distribution functions assuming, implicitly or explicitly, that the structure is isotropic.

* Corresponding authors.
E-mail addresses: peihao.sun@unipd.it (P. Sun), jbh@slac.stanford.edu (J.B. Hastings), giulio.monaco@unipd.it (G. Monaco).

https://doi.org/10.1016/j.mtla.2023.101847
Received 13 April 2023; Accepted 6 July 2023
Available online 7 July 2023

In this work, we perform X-ray diffraction with a nano-focused beam to study the local structure of a vapor-deposited metallic glass on length scales of tens of nanometers and above. The combined use of hard X-ray nano-beams and large-area 2D X-ray pixel detectors, both of which only became available in recent years, allows structural characterization on length scales that were previously inaccessible. We show that structural anisotropy can exist even at the length scales of tens of nanometers and above in an amorphous sample. Furthermore, with annealing near the glass transition temperature, T_g, the anisotropy disappears before the onset of crystallization. The experimental observations allow us to exclude alternative explanations of the anisotropy such as geometric effects, local strain, and nano-crystallization, leading to the conclusion that the anisotropy must arise from structural correlations within the as-deposited sample. We discuss the nature of the anisotropy as well as its significance for the understanding of the structural and thermodynamic properties of amorphous systems.

The samples are $Pd_{77.5}Cu_6Si_{16.5}$ (at.%) metallic glasses which are vapor-deposited onto a polished single-crystal NaCl substrate at a deposition rate of 1 nm/s. The substrate temperature is kept around $0.80T_g$ to $0.85T_g$. The deposited sample thickness is about 5 μm. After deposition, either the NaCl substrate is dissolved in pure water to obtain a free-standing sample or the sample is detached manually from the substrate (see Ref. [10] for more details).

The X-ray nano-diffraction experiment was performed at the nanofocus extension of beamline ID13 at the European Synchrotron Radiation Facility (ESRF, Grenoble, France) [11]. A schematic diagram of the setup is shown in Fig. 1. X-rays with a photon energy of 13 keV are focused by a pair of multilayer Laue lenses (MLLs) in a crossed geometry onto the sample plane [12]. The focus size is estimated to be around 60 nm × 60 nm (full width at half maximum) using a 2D transmission scan on a high-resolution X-ray chart with Ta absorbers of 50 nm minimum pattern size. The samples are mounted in transmission geometry. The sample volume illuminated by X-rays at each position is thus on the order of 60 nm × 60 nm × 5 μm. The flux in the focal plane is estimated to be around 3×10^{11} photons per second (at I = 200 mA electron beam current) based on measurements from a cross calibrated diode. An EIGER 4M detector (DECTRIS, Baden-Daettwill, Switzerland) is placed 70 mm behind the sample, perpendicular to the X-ray path and centered around the beam. During a typical scan, the diffraction images are taken from a 2D grid on the sample as indicated in Fig. 1, with usually 1 s exposure time at each step. The magnitude of the scattering vector, Q, corresponding to the detector pixel array is calibrated by performing diffraction on a polycrystalline α-Al_2O_3 sample. The collected Debye–Scherrer rings were used to quantify the sample-detector distance, the tilt angle of the detector plane and the rotation angle of the tilt plane, using the known detector pixel size of 75 μm × 75 μm. Also shown in Fig. 1 is an example of a diffraction pattern from the $Pd_{77.5}Cu_6Si_{16.5}$ sample, where the first and second diffraction maxima are visible.

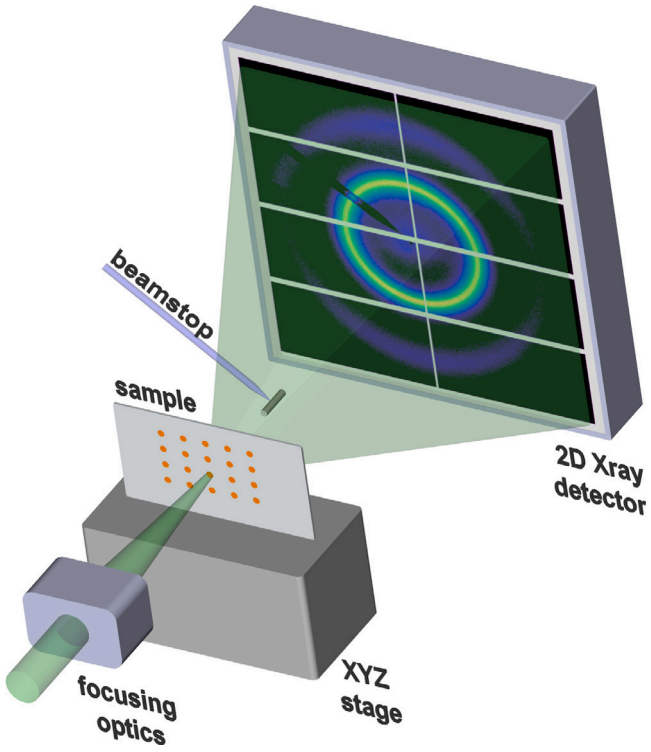

Fig. 1. Schematics of the experimental setup. 13 keV X-rays are focused onto the sample plane by a pair of MLLs. The diffracted X-rays are collected by an EIGER 4M detector placed 70 mm behind the sample and centered on the X-ray axis. During a typical scan, the sample is moved on a 2D grid as indicated by the yellow dots. Also shown is an example diffraction pattern from the vapor-deposited $Pd_{77.5}Cu_6Si_{16.5}$ sample.

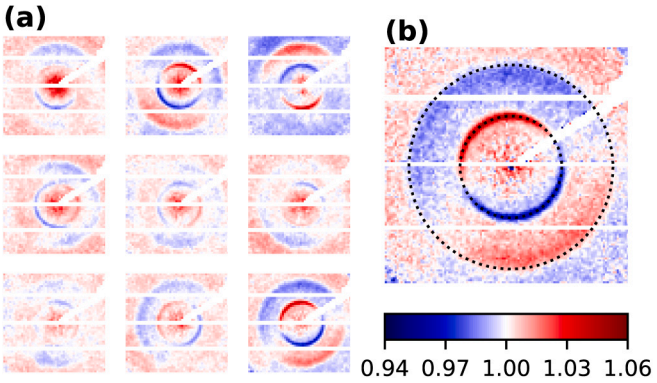

Fig. 2. Anisotropy in the as-deposited sample. (a) A subset of 9 images taken from a 2D scan. The variation along the azimuthal angle of the first diffraction ring can reach ±6%, see text for detailed information on how the images are obtained. (b) A magnified version of the last image of the subset, with dotted circles indicating the peak positions of the first and second diffraction rings. All images use the color bar shown on the bottom right.

Observation of local anisotropy. Fig. 2 shows an example of the anisotropy observed in the sample. Panel (a) shows 9 images taken from a 2D scan containing 31 × 31 steps with 100 nm step size. To obtain these plots, starting from each diffraction image, we first subtract an air scattering background which is measured without the sample. Next, the image is normalized by the average intensity around the first diffraction ring (from 2 $Å^{-1}$ to 4 $Å^{-1}$). Finally, we divide each image by the average of all 961 images in the scan. A small part of each image is masked (due to inactive detector area or shadowing of the beam stop) and shown as white.

It is clear from Fig. 2 that the intensity is not uniform around the first diffraction ring. In other words, the diffraction patterns are anisotropic, suggesting that the structure in the illuminated volume is anisotropic as well. Note that overall intensity modulations which affect all images, such as the polarization factor, are canceled out when dividing by the average image. The anisotropy changes between different positions on the sample and often reaches ±6% from the average image. In most cases, there is a single maximum and minimum around the ring, situated opposite from each other. We note in passing that this observation does not violate Friedel symmetry, because the diffraction angle corresponding to the first ring is about 25°, and thus the momentum transfer vectors **Q** that are 180° apart on the ring are far from opposite to each other (see also Supplementary Material). Close to the second ring, the polarity becomes opposite to that of the first ring—at the azimuthal angle where the intensity of the first ring is higher than average (red-colored), the intensity on the inner side of the second ring

is lower than average (blue-colored), and vice versa. This can be seen more easily in the magnified image in Fig. 2b, where the peak positions of the first and second diffraction rings are indicated by dotted circles. These observations are further discussed below.

It should be emphasized that the anisotropy is local, i.e., that it changes depending on the position on the sample. Therefore, the use of a small beam is crucial, as the effects could easily average out when a large area on the sample is illuminated. We have confirmed this during another experiment conducted at beamline BL19LXU at the SPring-8 synchrotron facility (Japan)—by moving the sample out of focus to achieve an approximately 11 μm × 9 μm beam size, the degree of anisotropy is reduced to less than 1% (see Supplementary Material for more details). This implies that local anisotropy may exist in other amorphous materials as well, but has evaded detection because the beam size is not small enough.

We note that similar observations can be made without the background subtraction and normalization procedure described above, although in this case, slight changes in sample thickness lead to overall intensity fluctuations in each image (see Supplementary Material Fig. S2). Therefore, the anisotropy is not an artifact of our analysis procedure. We have also confirmed that no X-ray-induced effects are observable in the diffraction patterns after at least 60 s of exposure (see Supplementary Material). Therefore, the 1 s exposure time used to acquire the images shown in Fig. 2 is sufficiently short to avoid radiation-induced artifacts.

Effects of annealing. Next, we investigate effects of annealing on the anisotropy. The annealing is done with the following procedure: the sample is first heated at a rate of 20 K/min from room temperature to the annealing temperature, T_a, then kept at T_a for 10 min, and finally cooled down at 20 K/min. We used three annealing temperatures: 602 K, 629 K, and 639 K. Note that the glass transition temperature, T_g, of $Pd_{77.5}Cu_6Si_{16.5}$ bulk metallic glasses is reported to be 636 K in Ref. [13] and 621 K in Ref. [14], so the chosen T_a values range from somewhat below T_g to slightly above it. After annealing, X-ray nanodiffraction is performed on the sample using the same method as for the as-deposited sample.

In Fig. 3 we show a subset of four images for each T_a. To facilitate comparison, the plots use the same color map as in Fig. 2. From Fig. 3, it is clear that the degree of anisotropy decreases significantly after annealing at 602 K, although a small amount still remains. With T_a = 629 K, the anisotropy is no longer observable. Finally, after annealing at 639 K, small Bragg peaks start to emerge (they appear as small red dots in these images), suggesting the formation of small crystallites. Thus we observe that, with increasing T_a, the anisotropy first decreases, then disappears, before crystallization takes place.

Alternative explanations? Before further discussions, it is important to exclude spurious or trivial effects which could have caused the anisotropic diffraction patterns: (1) Factors external to the sample, such as the experimental setup or detector artifacts, can be excluded because the anisotropy changes upon annealing. (2) We exclude geometric effects related to sample morphology (e.g., surface roughness or undulations, or bubble inclusions) because thickness variations on the μm scale are needed for ±6% intensity variations in this 5 μm sample, and more importantly because it is improbable that geometric effects are always associated with the first and second rings (more details are shown in the Supplementary Material). (3) Local strain is excluded because it should be associated with a change in the Q position in the first peak [15,16], while no such shifts are observed (more details are shown in the Supplementary Material). (4) It is unlikely that the anisotropy exists only close to the surface, because ±6% intensity variation on a 5 μm sample implies that the anisotropic thickness should be at least tens or hundreds of nm. (5) Small crystallites are excluded as the origin because no Bragg peaks are observed in the as-deposited sample, and because crystallites are expected to grow with annealing instead of disappearing [17]. Similarly, nanophase separation can be excluded as it is expected to be enhanced by annealing [17]. However, it is possible that nano-scale crystallite-like structures exist in the sample, conceptually similar to Ref. [3]; this is indeed our interpretation, as will be further discussed below.

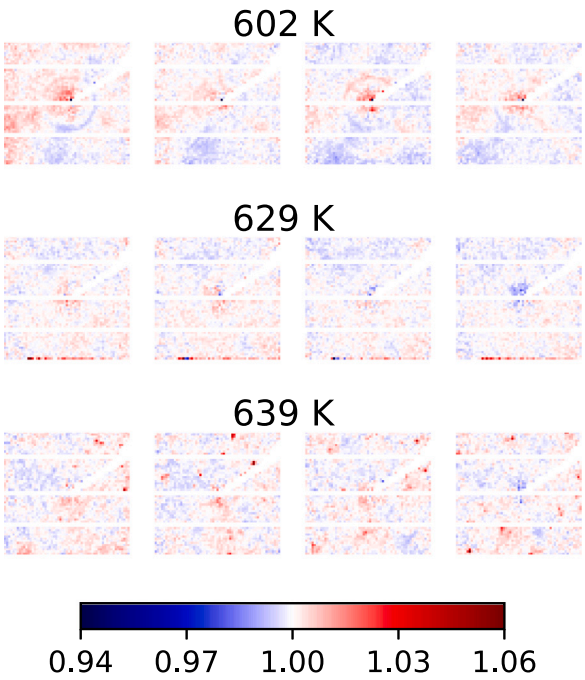

Fig. 3. Effects of annealing. Each row corresponds to a different annealing temperature T_a, as indicated in the title. The color map is the same as in Fig. 2. The anisotropy becomes weaker for T_a = 602 K, disappears for T_a = 629 K, and weak Bragg peaks begin to appear for T_a = 639 K.

Previous observations of anisotropy in thin-film metallic glasses. Notably, structural anisotropy has been observed in vapor-deposited thin-film metallic glass samples in earlier studies [18–20], and it is worth discussing its relation to the present results. Firstly, we note that in the earlier studies, the anisotropy is between in-plane and out-of-plane directions [18–20]. In our study, instead, the probed **Q** vectors are mostly in-plane (**Q** forms a mere 12.4° angle with the sample plane), and, assuming that the sample is flat, the magnitudes of the in- and out-of-plane components remain the same during the scans. In other words, what we observe is structural anisotropy among different in-plane directions which changes between different positions on the sample. Moreover, the anisotropy observed by Yan et al. [18] shows up as a shift in the center Q position of the first peak. In contrast, as mentioned above, the anisotropy in this study does not appear as a shift in the center Q position of the first peak, but rather its amplitude. Therefore, our observation differs from those reported before. We note in passing that no in- and out-of-plane anisotropy in the Q position of the first diffraction peak is observed in our sample (see Supplementary Material).

Nature of the anisotropy. We now discuss possible origins of the anisotropy. To begin with, we note that for anisotropy to exist in a macroscopic volume, there must be a microscopic structural origin. In other words, there must exist some anisotropic local structures in the sample, which are likely MRO units. While the existence of MRO in metallic glasses is widely accepted nowadays [5], our observations nonetheless present several unusual aspects.

Firstly, for the anisotropy to appear in the diffraction patterns, the anisotropic local structures must have a way to align with each other, because otherwise they would easily average out within the large probed volume of around 60 nm × 60 nm × 5 μm. This means that they

probably exist contiguously within the sample volume: if instead they are embedded within a network of isotropic random structure, their orientations should also be random, as it appears to be the case for monolayer amorphous carbon as shown in a recent work [3]. Therefore, the anisotropic local units likely span the sample volume and are the predominant structural motif.

Secondly, the maximum and minimum around the first ring usually appear opposite to each other, as can be seen in Fig. 2. This suggests that within each probed volume, there is usually a single preferred orientation for the anisotropic MRO units. Conceptually, this may be similar to texture in a polycrystalline sample. Indeed, it is known that vapor-deposited polycrystalline samples can become strongly textured through various mechanisms [21], for example via surface energy minimization at high substrate temperatures. Some of these mechanisms might apply to our sample as well.

Even more interesting are observations related to the second ring, as can be seen clearly in Fig. 2b: (i) at the center of the second peak indicated by the dotted circle, the values are close to unity; (ii) the inner and outer sides of the second peak deviate from 1 in opposite directions, which show up as different colors (red vs blue); (iii) at the same azimuthal angle, the inner side of the second ring almost always shows the opposite color from the first ring. Observations i and ii together indicate that it is the center Q position of the second peak, rather than its peak amplitude, which changes around the azimuth. Note that the contrary is true for the first peak, where it is the amplitude and not the center Q position that changes. Regarding observation iii, it is known that for metallic glasses in general, the first peak in $S(Q)$ is mostly associated with medium-range correlations (second coordination shell and above) [22], while the second peak and above are more influenced by the SRO. Therefore, observation iii suggests that in the preferred direction of the MRO (stronger first peak), the SRO is also somewhat more compact (the second peak moves to slightly higher Q), and vice versa. However, the exact structural details cannot be determined based on the present results and may be a subject for further studies.

Finally, we discuss possible physical mechanisms for the observed behavior of the sample. We note that, although metallic glass samples that are vapor-deposited onto cold substrates are observed to exhibit structural relaxation upon annealing [23], the sample in this study is deposited at an elevated substrate temperature ($0.80T_g$ to $0.85T_g$); similarly prepared samples have been observed to exhibit higher mechanical stability [10] and slower dynamics [24]. Furthermore, the anisotropy in the as-deposited sample suggests a high degree of ordering, which seems to disappear upon annealing. These observations may appear self-contradictory if one draws the usual conclusion that annealing leads to structural relaxation and enhanced ordering. However, they could be explained by the possible existence of two disordered states with the same composition, and with annealing the sample may transition from one state to another. This has indeed been proposed to explain the annealing behavior of a vapor-deposited Zr-based sample [25] (although in that case, the deposition was done at room temperature). In addition, recent simulation results show that in some metallic glass-forming liquids, a homogeneous, disordered liquid-like "L-phase" may freeze into a heterogeneous "G-phase" composed of locally ordered regions surrounded by disordered regions [26–28]. If such a transition does exist in $Pd_{77.5}Cu_6Si_{16.5}$, our results suggest that the as-deposited sample, which appears to exhibit a higher degree of ordering, corresponds to the ordered G-phase; the loss of anisotropy upon annealing close to T_g suggests a transition (partially or fully) into the disordered L-phase. Whether this is indeed the case is subject to confirmation by future studies.

In summary, using X-ray nano-diffraction on a vapor-deposited $Pd_{77.5}Cu_6Si_{16.5}$ sample, we have observed significant local anisotropy within each probed region of around 60 nm × 60 nm × 5 μm, which disappears after annealing. Our results indicate that, in the as-deposited sample: (1) there must exist local ordering, likely MRO; (2) this ordering should be the predominant structural motif in the sample; (3) there exist long-range correlations between the orientations of the locally ordered units. We emphasize that all of these occur within a sample which appears completely amorphous under X-ray diffraction. These peculiar properties point out the importance of local ordering and the need for new structural descriptions for metallic glasses.

Declaration of competing interest

The authors declare that they have no known competing financial interests or personal relationships that could have appeared to influence the work reported in this paper.

Data availability

Data related to this article can be found with http://dx.doi.org/10.17632/d3wy4ny7fr.1

Acknowledgments

We acknowledge the European Synchrotron Radiation Facility (ESRF) for provision of synchrotron radiation facilities and we would like to thank A. P. Melnikov and M. Burghammer for assistance and support in using beamline ID13, and J.-P. Suuronen and R. Tucoulou for assistance and support in using beamline ID16B. A part of this work was performed at BL19LXU of SPring-8 with the approval of the Japan Synchrotron Radiation Research Institute (JASRI) (Proposal No. 20190037), and we thank K. Tamasaku and H. Ohsumi for their help. We also thank Chuntian Cao and Michael Toney for their help at beamline 11–3 at the Stanford Synchrotron Radiation Lightsource (SSRL). This project has received funding from the European Union's Horizon 2020 research and innovation programme under the Marie Skłodowska-Curie grant agreement No. 101023787. This work has also been supported by the US DOE, Office of Science, Office of Basic Energy Sciences, USA under Contract DE-AC02-76SF00515, and by the National Science Centre, Poland, Grant Agreement 2017/27/B/ST3/02860. F. Caporaletti is a chargé de recherches of the Fonds de la Recherche Scientifique – FNRS.

Appendix A. Supplementary data

Supplementary material related to this article can be found online at https://doi.org/10.1016/j.mtla.2023.101847.

References

[1] W.H. Zachariasen, The atomic arrangement in glass, J. Am. Chem. Soc. 54 (10) (1932) 3841–3851, http://dx.doi.org/10.1021/ja01349a006.

[2] J.D. Bernal, Geometry of the structure of monatomic liquids, Nature 185 (4706) (1960) 68–70, http://dx.doi.org/10.1038/185068a0.

[3] C.-T. Toh, H. Zhang, J. Lin, A.S. Mayorov, Y.-P. Wang, C.M. Orofeo, D.B. Ferry, H. Andersen, N. Kakenov, Z. Guo, I.H. Abidi, H. Sims, K. Suenaga, S.T. Pantelides, B. Özyilmaz, Synthesis and properties of free-standing monolayer amorphous carbon, Nature 577 (7789) (2020) 199–203, http://dx.doi.org/10.1038/s41586-019-1871-2.

[4] H.W. Sheng, W.K. Luo, F.M. Alamgir, J.M. Bai, E. Ma, Atomic packing and short-to-medium-range order in metallic glasses, Nature 439 (7075) (2006) 419–425, http://dx.doi.org/10.1038/nature04421.

[5] Y. Cheng, E. Ma, Atomic-level structure and structure–property relationship in metallic glasses, Prog. Mater. Sci. 56 (4) (2011) 379–473, http://dx.doi.org/10.1016/j.pmatsci.2010.12.002.

[6] P.S. Salmon, R.A. Martin, P.E. Mason, G.J. Cuello, Topological versus chemical ordering in network glasses at intermediate and extended length scales, Nature 435 (7038) (2005) 75–78, http://dx.doi.org/10.1038/nature03475.

[7] S. Hilke, H. Rösner, G. Wilde, The role of minor alloying in the plasticity of bulk metallic glasses, Scr. Mater. 188 (2020) 50–53, http://dx.doi.org/10.1016/j.scriptamat.2020.06.070.

[8] Z.P. Lu, C.T. Liu, Role of minor alloying additions in formation of bulk metallic glasses: A Review, J. Mater. Sci. 39 (12) (2004) 3965–3974, http://dx.doi.org/10.1023/B:JMSC.0000031478.73621.64.

[9] Q. Zeng, H. Sheng, Y. Ding, L. Wang, W. Yang, J.-Z. Jiang, W.L. Mao, H.-K. Mao, Long-range topological order in metallic glass, Science 332 (6036) (2011) 1404–1406, http://dx.doi.org/10.1126/science.1200324.

[10] H.-B. Yu, Y. Luo, K. Samwer, Ultrastable metallic glass, Adv. Mater. 25 (41) (2013) 5904–5908, http://dx.doi.org/10.1002/adma.201302700.

[11] C. Riekel, M. Burghammer, R. Davies, Progress in micro- and nano-diffraction at the ESRF ID13 beamline, IOP Conf. Ser.: Mater. Sci. Eng. 14 (2010) 012013, http://dx.doi.org/10.1088/1757-899X/14/1/012013.

[12] A. Kubec, K. Melzer, J. Gluch, S. Niese, S. Braun, J. Patommel, M. Burghammer, A. Leson, Point focusing with flat and wedged crossed multilayer Laue lenses, J. Synchrotron Radiat. 24 (2) (2017) 413–421, http://dx.doi.org/10.1107/S1600577517001722.

[13] H.S. Chen, The influence of structural relaxation on the density and Young's modulus of metallic glasses, J. Appl. Phys. 49 (6) (1978) 3289–3291, http://dx.doi.org/10.1063/1.325279.

[14] K.-F. Yao, Y.-Q. Yang, N. Chen, Mechanical properties of Pd–Cu–Si bulk metallic glass, Intermetallics 15 (5–6) (2007) 639–643, http://dx.doi.org/10.1016/j.intermet.2007.03.005.

[15] H.F. Poulsen, J.A. Wert, J. Neuefeind, V. Honkimäki, M. Daymond, Measuring strain distributions in amorphous materials, Nature Mater. 4 (1) (2005) 33–36, http://dx.doi.org/10.1038/nmat1266.

[16] T.C. Hufnagel, R.T. Ott, J. Almer, Structural aspects of elastic deformation of a metallic glass, Phys. Rev. B 73 (6) (2006) 064204, http://dx.doi.org/10.1103/PhysRevB.73.064204.

[17] D. Kim, W. Kim, E. Park, N. Mattern, J. Eckert, Phase separation in metallic glasses, Prog. Mater. Sci. 58 (8) (2013) 1103–1172, http://dx.doi.org/10.1016/j.pmatsci.2013.04.002.

[18] X. Yan, M. Hirscher, T. Egami, E.E. Marinero, Direct observation of anelastic bond-orientational anisotropy in amorphous $Tb_{26}Fe_{62}Co_{12}$ thin films by X-ray diffraction, Phys. Rev. B 43 (11) (1991) 9300–9303, http://dx.doi.org/10.1103/PhysRevB.43.9300.

[19] V.G. Harris, K.D. Aylesworth, B.N. Das, W.T. Elam, N.C. Koon, Structural origins of magnetic anisotropy in sputtered amorphous Tb-Fe films, Phys. Rev. Lett. 69 (13) (1992) 1939–1942, http://dx.doi.org/10.1103/PhysRevLett.69.1939.

[20] T.C. Hufnagel, S. Brennan, P. Zschack, B.M. Clemens, Structural anisotropy in amorphous Fe-Tb thin films, Phys. Rev. B 53 (18) (1996) 12024–12030, http://dx.doi.org/10.1103/PhysRevB.53.12024.

[21] S. Mahieu, P. Ghekiere, D. Depla, R. De Gryse, Biaxial alignment in sputter deposited thin films, Thin Solid Films 515 (4) (2006) 1229–1249, http://dx.doi.org/10.1016/j.tsf.2006.06.027.

[22] G. Cargill, Structure of metallic alloy glasses, Solid State Phys. -Adv. Res. Appl. 30 (1975) 227–320, http://dx.doi.org/10.1016/S0081-1947(08)60337-9.

[23] Y.H. Liu, T. Fujita, D.P.B. Aji, M. Matsuura, M.W. Chen, Structural origins of Johari-Goldstein relaxation in a metallic glass, Nature Commun. 5 (1) (2014) 3238, http://dx.doi.org/10.1038/ncomms4238.

[24] M. Lüttich, V.M. Giordano, S. Le Floch, E. Pineda, F. Zontone, Y. Luo, K. Samwer, B. Ruta, Anti-aging in ultrastable metallic glasses, Phys. Rev. Lett. 120 (13) (2018) 135504, http://dx.doi.org/10.1103/PhysRevLett.120.135504.

[25] Q. Sun, D.M. Miskovic, H. Kong, M. Ferry, Transition from relaxation to rejuvenation in ultrastable metallic glass driven by annealing, Appl. Surf. Sci. 546 (2021) 149048, http://dx.doi.org/10.1016/j.apsusc.2021.149048.

[26] J.H. Na, S.L. Corona, A. Hoff, W.L. Johnson, Observation of an apparent first-order glass transition in ultrafragile Pt–Cu–P bulk metallic glasses, Proc. Natl. Acad. Sci. 117 (6) (2020) 2779–2787, http://dx.doi.org/10.1073/pnas.1916371117.

[27] Q. An, W.L. Johnson, K. Samwer, S.L. Corona, W.A. Goddard, Formation of two glass phases in binary Cu-Ag liquid, Acta Mater. 195 (2020) 274–281, http://dx.doi.org/10.1016/j.actamat.2020.05.060.

[28] S.L. Corona, Emerging Evidence of a Second Glass Phase in Strong to Ultra-Fragile Bulk Metallic Glass-Forming Liquids (Ph.D. thesis), California Institute of Technology, Pasadena, California, 2022, http://dx.doi.org/10.7907/9bvb-2d78, https://thesis.library.caltech.edu/14545.